DOI: https://doi.org/10.14311/TPFM.2020.008

INDIVIDUAL VORTEX SEARCHING ALGORITHM

D. Duda [1]

[1] **Department of Power System Engineering, Faculty of Mechanical Engineering, University of West Bohemia in Pilsen, Univerzitní 22, 306 14 Pilsen, Czech Republic**

Abstract

The turbulent flows consist of vortices and other coherent structures, whose motion is such highly ordered, that it is usually considered to be random. We try to bring light into this problem by using the ideas coming from research of superfluid flows, where the turbulence consists of quantized vortices – linear topological singularities in the macroscopic order parameter.

We present an algorithm developed for searching of individual vortices in an experimentally obtained 2D flow-field of a classical fluid (e.g. air). This algorithm directly fits the flow-field by the Gauss's model of vortex minimizing energy of the rest. The statistics of the reconstructed vortices can help us to understand the turbulence from another point of view.

Keywords: Particle Image Velocimetry, Turbulence, Vortex.

1 Introduction

The parallel between the *classical* and the *quantum* hydrodynamics at *large* length-scales [1] suggests, that the standard *mesoscopic* description of turbulence is insufficient. This description is represented by the continuum hypothesis and the *Navier-Stokes equations* [2] in the case of classical hydrodynamics; in the case of quantum hydrodynamics, this level of description is covered by the *Landau two-fluid equations* [3] and the tangle of quantized vortices [4]. These models are cardinally different, which is apparent from experimental data at corresponding length-scale [5]. On the other hand, at larger length-scales both converge to the common CLASSICAL REGIME [1], although, the only thing, which is common for both systems, is the interaction between *vortices*. Of course, the description of vortices is absolutely different – quantized vortices have core of infinitesimal cross-section and they cannot directly dissipate. In the case of classical hydrodynamics, the interactions between vortices are responsible for the famous Richardson Cascade and the power spectrum of $k^{-5/3}$. In the quantum turbulence is this spectrum produced by the *polarized part* of vortex tangle [6, 7, 8].

In the case of classical hydrodynamics, the vortex is much more difficult to describe. The Helmholtz theorems *does not apply*. Additionally, the circulation and core size have no limits. And even the vortex core itself can become turbulent containing other vortices [9].

Due to this, there is no any rigid definition of vortex up to nowadays [10], even not for the simplest case of a two-dimensional flow field. In the Next, we will focus only to the two-dimensional cuts of velocity fields, which is an outcome of the experimental technique PIV (Particle Image Velocimetry).

In order to bring new light into the experimental investigation of turbulence we try to develop an algorithm for identification of individual vortices in an experimentally obtained two-dimensional velocity field. This algorithm is under development and in this paper we discuss some of the technical aspects, which can seem to be secondary, but whose tuning affects the outcome quality. It is important to understand the tools we are using in order to not mismatch the properties of studied phenomena and those of the used method.

2 Sample data

The data used in this paper are measured by using the PIV (Particle Image Velocimetry) system from company Dantec at the University of West Bohemia. The free turbulent flow is obtained in a wake past a grid of square rods mounted in a open low-speed wind tunnel, see figure 1.

The PIV measurement is based on optical observing of small particles carried by the flow [11, 12]. The tracer particles are produced by a commercially available fog generator Safex, whose usage

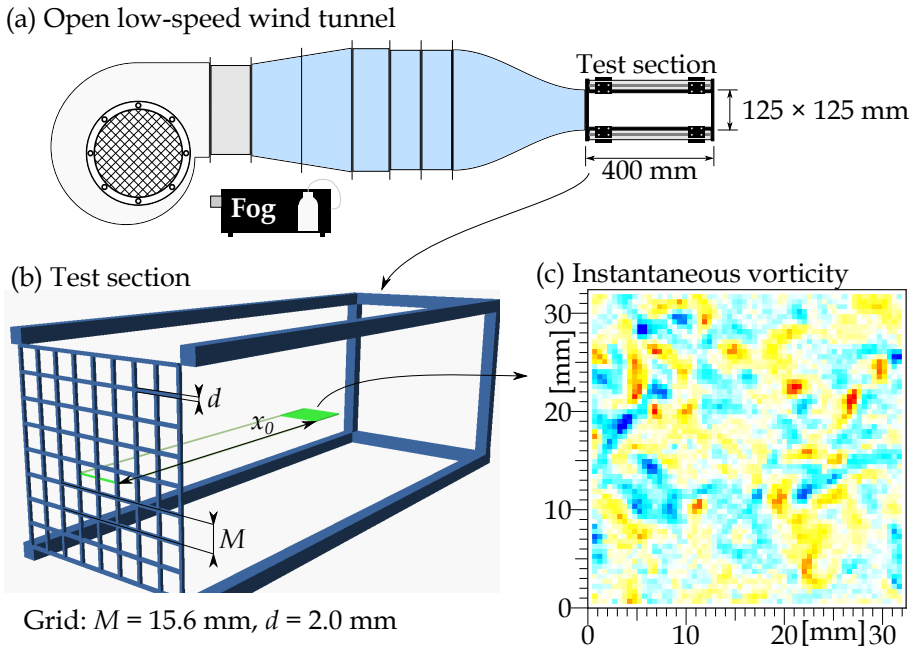

Figure 1: Experimental setup: grid (b) is mounted at inlet into a test section of an open low-speed wind tunnel (a). The studied area has size $32 \times 32\,\mathrm{mm} \approx 2 \times 2M$ and it is located at distance $x_0 = 200\,\mathrm{mm} \approx 12.8M$ from the grid. The stream-wise orientation is projected into direction x, while one of the span-wise directions does into y; the second span-wise component is not measured. The plane of studied area lies 7.5 mm under the test-section axis, which is behind the holes, not behind rods (but at these distances it *should be* irrelevant). Panel (c) shows an example of instantaneous vorticity field at stream-wise velocity $U = 6.0\,\mathrm{m/s}$, i.e. $\mathrm{Re}_M \approx 6.3 \cdot 10^3$.

for air has been proven by experience [13, 14, 15]. The particles are illuminated by a solid-state laser New Wave Solo and captured by a double-frame camera FlowSense MkII. The rough images are processed by using function Adaptive PIV in software Dantec Dynamic Studio. Resulted vector fields are then exported and further processed by a custom-made software described in this article.

The experimental data used for showing the features of our software are taken in *grid turbulence*[16], which is generally tough to be homogeneous and isotropic example of ideal Kolmogorov-type turbulence [17].

The grid is located at the inlet into a test section of an open low-speed wind tunnel. The quality of incoming flow is achieved by using a honey-comb plate, by a pair of fine grid plates and by accelerating in a nozzle. The schematic sketch of our wind tunnel is drawn in figure 1. The test section is 400 mm long and its cross-sectional size is 125×125 mm. The studied grid has rods of square cross-section with side-size $d = 2$ mm; the distance of these rods is $M = 125/8 = 15.625$ mm, therefore the porosity

$$\beta = \frac{\text{free area}}{\text{total area}} = \frac{(M-d)^2}{M^2} = 0.76. \tag{1}$$

In the grid turbulence, M is taken as a main length-scale, therefore we define the Reynolds number Re_M by using this length

$$\mathrm{Re}_M = \frac{UM}{\nu} = 6.3 \cdot 10^3, \tag{2}$$

where $U = 6.0\,\mathrm{m/s}$ is the average stream-wise velocity and ν is the kinematic viscosity of air, $\nu = 1.5 \cdot 10^{-5}\,\mathrm{m^2/s}$. The studied area has size 32×32 mm, which corresponds to $2M$ and it located in the distance $x_0 = 200\,\mathrm{mm} = 12.8M$ from the grid. The stream-wise direction lies inside this plane. We are measuring only two velocity components, the first, denoted u is the stream-wise one, the perpendicular span-wise component is denoted v and the third component is not measured in

this experiment.

3 Preprocessing of the velocity field

The measured velocity field is dominated by a simple movement in stream-wise direction by the average velocity U. This component is energetically dominating, therefore, when we want to study turbulence, we have to remove this *laminar* component. We have written a lot about fluctuation decompositions, see e.g. [18]. Generally speaking, we have two main possibilities: remove the time-average, which is called *Reynolds decomposition*, or remove the spatial average. In the later, we have more freedom, we can use only a local average, represented by the Gaussian filter [19, 20], or we can remove the spatial average over the entire field of view. The last is the method used in this case, as we do not want to insert any artificial information about sizes of the flow-structures.

4 Fitting single vortex

We have a 2D velocity field, where we try to find a single vortex. This vortex has, in our approach, 4 fitting parameters: the position x and y, circulation Γ and radius of core R. Of-course, as we are working with a 2D cuts of 3D turbulent velocity fields, this set of parameters describes the cases, when the vortex tube crosses perpendicularly the studied plane, other angles might produce deformation of the ideal circular shape. But, as the John von Neumman said, *With four parameters I can fit an elephant, and with five I can make him wiggle his trunk* [21], therefore we prefer to avoid using too many fitting parameters.

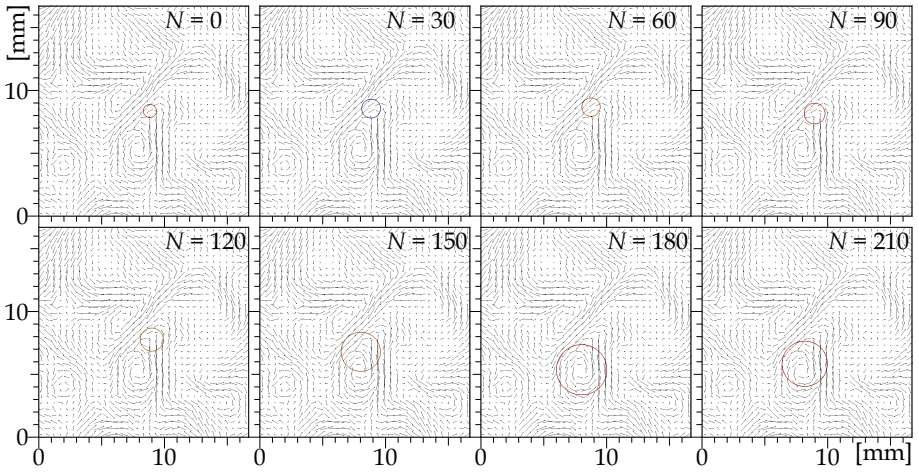

Figure 2: Example of steps of fitting procedure. The starting position of has been in the center of the Field of View, the starting radius was 1 IA. The number N in each panel indicates the number of calling the function for calculating the energy of the residual velocity field (it is approximately $3\times$ the number of calling the *Amoeba function*).

We used the algorithm called Amoeba, which is described in the book [22]. Of-course, a number of very effective fitting algorithms has been invented during years, but we chose this one, as it is very robust and quite easy to implement; the higher computational cost is not relevant, as our program is still under development. The algorithm uses a set of fitted variants, whose number is 1+ the number of fitting parameters ($4 + 1 = 5$ in our case), and it calculates the *score* of each variant. The score in our case is the energy of the residual velocity field, i.e. field, from which we subtract the vortex of given parameters. Then this algorithm selects one from a set of movements in order to keep away from areas with higher score and converging to a local minimum. The movement of a such set of points suggests the real amoeba, which bring a name to this algorithm.

Figure 2 shows the result of this procedure; the starting variant has been located in the center of the used field of view. At early stages, the algorithm *maps* the ambient trying also a not very

relevant positions, then it smells a trail and falls into a relevant minimum.

5 Fitting vortex field

Once we have a vortex of such parameters, that the energy of the residual velocity field is in local minimum, we subtract this vortex from the velocity field and repeat the procedure above.

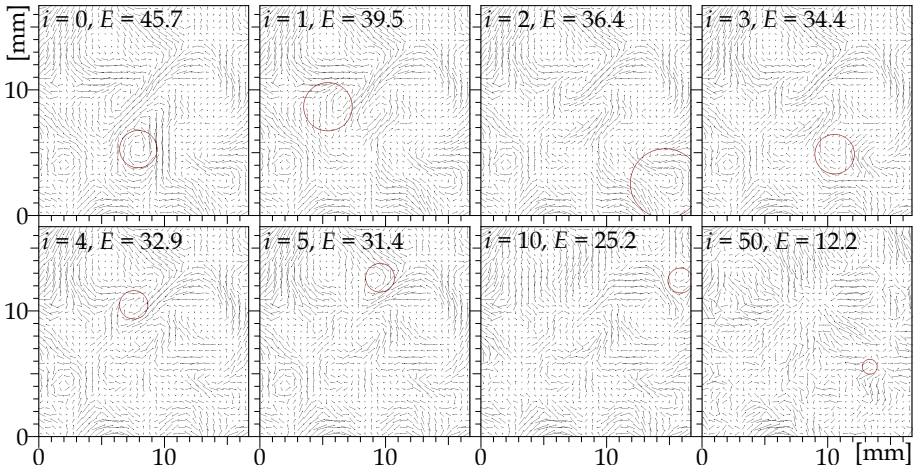

Figure 3: Vortices fitted in the sample velocity field. Energy E is in $\left[\mathrm{mm}^2\mathrm{s}^{-2}\right]$ and it means the kinetic energy of the displayed velocity field after subtracting the found vortex depicted as a red circle.

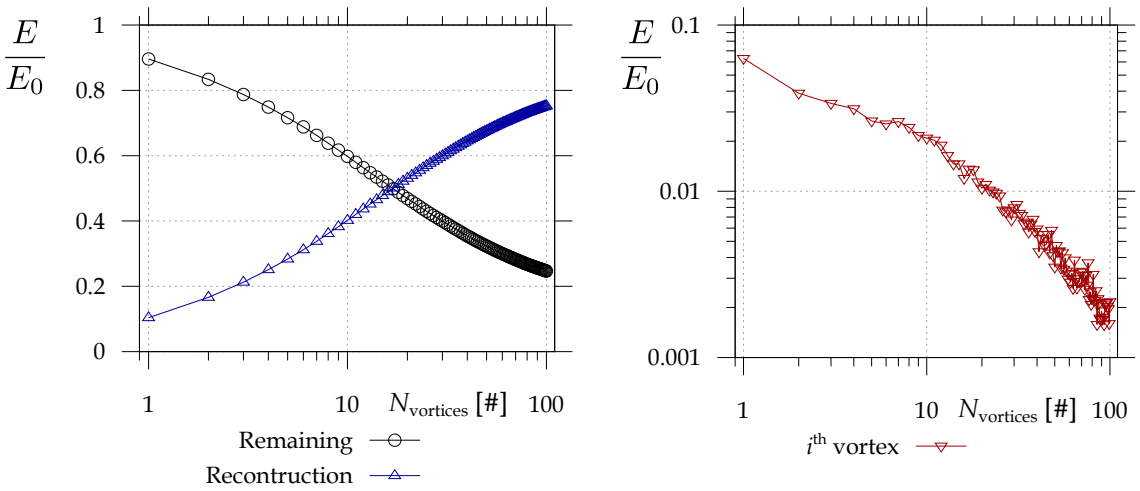

Figure 4: The energy of velocity field normalized by the energy of the original velocity field (after removing the stream-wise movement) as a function of the number of vortices fitted. **Black** ∘ represents the velocity field after subtracting the found vortex; **blue** Δ denotes velocity field reconstructed by using the found vortices and **red** ∇ plays for the velocity field of the actual vortex. The data are averaged over 1107 instantaneous velocity fields similar to that shown in figure 1c.

In figure 3 we can see, as the energy of the remaining velocity field decreases with number of removed vortices. Graph 4 shows this development on a statistical set of thousand instantaneous velocity fields.

Energy of the rest decreases with number of vortices much more slower than at other decomposition methods, such as the famous Proper Orthogonal Decomposition (POD) [23, 24, 25], where the remaining energy typically falls very rapidly with the number of used modes. On the other hand, the modes are mathematical structures produced statistically from the set – it is not possible to do that POD on a single velocity field. Additionally, the modes do not take place in the real data, while vortices are real physical objects having energy and momentum.

On the other hand, it does not converges fully – even for 100 vortices in a single instantenout field, we still cover about 75% of energy of the input velocity field. The remaining field contains divergent areas together with areas of uniform motion and some noisy background, see figure 5 for the insight to the reconstructed and remaining velocity fields.

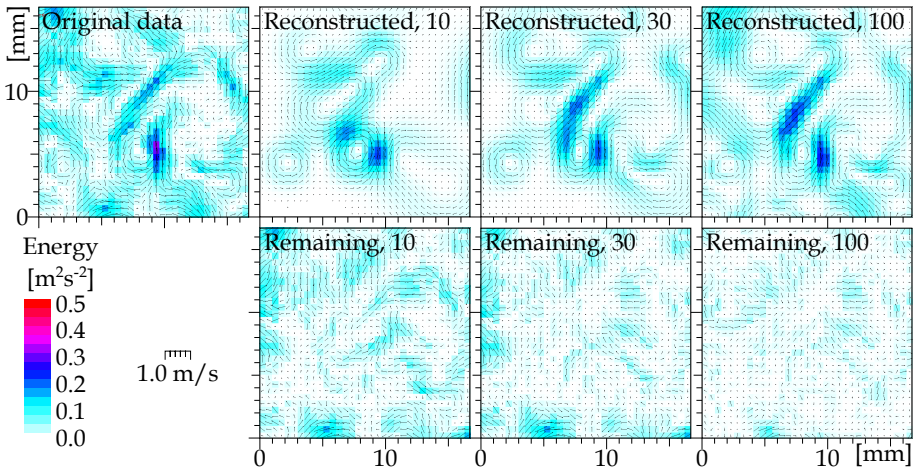

Figure 5: The reconstructed and remaining velocity field for 10, 30 and 100 vortices. The sample data shows only the center of the measured instantaneous velocity field, similarly as in previous figures.

6 Discussion

The fitting algorithm has to start from some location (and radius and circulation) of the vortex. Ideally, this starting point might not affect the results, but the convergence is better, when we start close to some real vortex.

The choice of starting parameters of the fit uses the maximum of some appropriate scalar property determined from the velocity field. Looking for a reasonable scalar parameter, which would indicate vortex, is a often quest of other studies; a list can be found in work of Holmén [26].

Probably the best method offers the *triple decomposition* of Kolář [27], which is computationally very time-consuming. Additionally, finding of the eigen axes of velocity gradient tensor suggested in [28] is too complicated quest for me.

The basic scalar parameter is the vorticity

$$\omega = \nabla \times \vec{u} \tag{3}$$

This scalar parameter has a often cited disadvantage, that it does not distinguishes vortices and shear layers [29], which is a serious problem even during fitting. The example of vorticity distribution is shown in figure 6(a).

We have tried also a less local methods, which are less sensible to the noise. One of this is the scalar convolution with the vortex model of a rigid radius $R = 2\,\mathrm{IA}$

$$C_G(\vec{x}) = \int \vec{u}(\vec{x}+\vec{y}) \cdot \vec{V}_G(\vec{y})\,\mathrm{d}\vec{y}, \tag{4}$$

where $\vec{V}_G(\vec{x})$ is the velocity around a Gauss's vortex. An example is shown in figure 6(b).

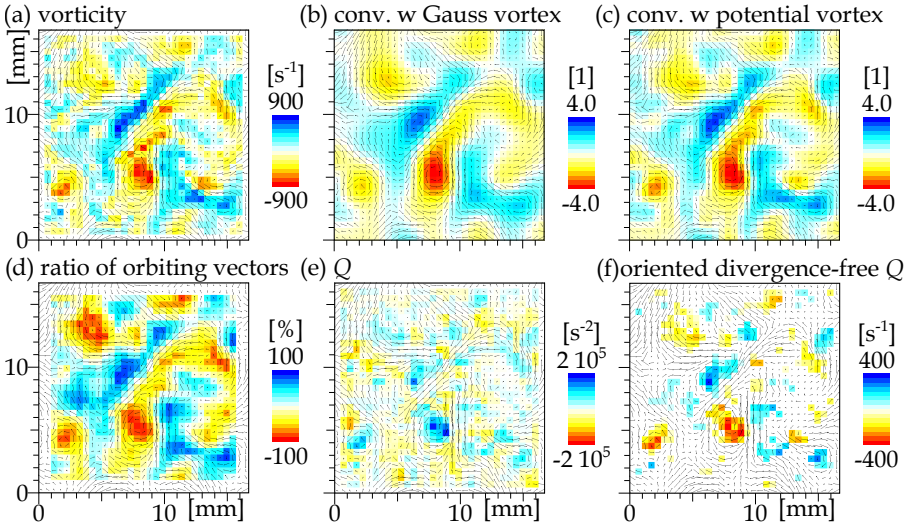

Figure 6: Examples of scalar parameters, which can be used as a starting point for vortex fitting. **(a)** vorticity, **(b)** convolution with Gauss's vortex model of constant core radius $R = 2\,\mathrm{IA}$, **(c)** convolution with potential vortex envelope, **(d)** amount of vectors, which are oriented clock-wise in the vicinity of the probed point, **(e)** Q, second invariant of the velocity gradient tensor, **(f)** square root of Q with subtracted divergence oriented according to vorticity (Q itself loss the information about vortex orientation).

A quantity, which is independent on the artificial parameter of core radius, is the convolution with the potential vortex envelope

$$C_P\left(\vec{x}\right) = \int \vec{u}\left(\vec{x}+\vec{y}\right)\cdot\vec{V}_P\left(\vec{y}\right)\mathrm{d}\vec{y}. \tag{5}$$

Example of this scalar parameter is displayed in figure 6(c).

A pure topological scalar parameter suggests Agrawal in article [30, 19]. He suggests to use the ratio of surrounding vectors, which points in the same tangential direction. An advantage of this approach is, that it shows weak vortices as well as strong ones, on the other hand, it is also sensitive to shear. This ratio is shown in figure 6(d).

The method for removing shear effects is the second invariant of velocity gradient tensor

$$Q = \frac{1}{2}\left(\omega^2 - s^2\right) = \frac{1}{2}\left(\mathrm{Tr}^2\nabla\vec{u} - \mathrm{Tr}\left(\nabla\vec{u}\right)^2\right), \tag{6}$$

where $\mathrm{Tr}\nabla\vec{u}$ is the *trace* of velocity gradient tensor $\nabla\vec{u}$, or its second power respectively. The negative value of Q highlights areas dominated by shear s, while the positive ones do areas dominated by vorticity ω. Spatial map of Q is shown in figure 6(e). This parameter alone is not ideal as it loss the information about the vortex orientation, therefore we accept only the positive part, which we square root and the multiply by signum of vorticity in order to return the information about vortex orientation.

During the fitting process, there start to be dominant the divergent areas, see figure 3. This issue is usually not reported in the literature, because it is prohibited by continuity equation. But we are working with 2D cuts of 3D velocity field, where divergence is not a problem – it means, that the fluid rounds perpendicularly. Q itself is quite sensitive to the divergence, thus we subtract the divergence in a same manner as shear:

$$Q_d = \frac{1}{2}\left(\omega^2 - s^2 - d^2\right) \tag{7}$$

$$q_d^{or} = \sqrt{\left(Q_d^+\right)}\cdot\mathrm{sign}\omega. \tag{8}$$

We found that the fitting procedure converges fastest when using this scalar parameter as the starting point. Its example is shown in figure 6.

7 Conclusion

We have developed an algorithm for direct vortex fitting of the experimentally obtained 2D velocity fields. This method can be used for reconstruction of velocity field with less information, but its effectivity is far from the robust pure mathematical methods like *proper orthogonal decomposition* POD. But our basis functions represent real physical objects – Gauss vortices, whose parameters can bring light into the still mysterious problem of turbulence.

Future work will be focused on the statistical processing of the parameters of found vortices and the physical interpretation of those results. We also plan to analyze data of Stereo-PIV (three velocity components in a 2D plane).

Acknowledgment

The financial support for the present project was partly provided by the student Project SGS-2019-021 (Improving the efficiency, reliability and service life of power machines and equipment 5).
Author thanks to prof. Václav Uruba for valuable discussions, to Dr. Vitalii Yanovych for technical help and to Ing. Pavel Žitek for new camera lens.

References

[1] La Mantia, M. & Švančara, P. & Duda, D., & Skrbek, L.: Small-scale universality of particle dynamics in quantum turbulence. *Physical Review B*, vol. 94 no. 18: (2016).

[2] Richardson, L. F.: Atmospheric diffusion shown on a distance-neighbour graph. *Proceedings of the Royal Society A: Mathematical, Physical and Engineering Sciences*, vol. 10 no. 756: (1926) pp. 709–737.

[3] Vinen, W. F.: An introduction to quantum turbulence. *Journal of Low Temperature Physics*, vol. 145 no. 1-4: (2006) pp. 7–24.

[4] Barenghi, C. F. & Skrbek, L., & Sreenivasan, K. R.: Introduction to quantum turbulence. *Proceedings of National Academy of Sciences of the United States of America*, vol. 111 (2014) pp. 4647–4652.

[5] Fonda, E. & Meichle, D. P. & Ouellette, N. T. & Hormoz, S., & Lathrop, D. P.: Direct observation of Kelvin waves excited by quantized vortex reconnection. *Proceedings of the National Academy of Sciences*, vol. 111 no. Supplement_1: (2014) pp. 4707–4710.

[6] Baggaley, A. W. & Laurie, J., & Barenghi, C. F.: Vortex-density fluctuations, energy spectra, and vortical regions in superfluid turbulence. *Physical Review Letters*, vol. 109 no. 20: (2012).

[7] Barenghi, C. F. & Sergeev, Y. A., & Baggaley, A. W.: Regimes of turbulence without an energy cascade. *Scientific Reports*, vol. 6 (2016) pp. 1–11.

[8] Cooper, R. G. & Mesgarnezhad, M. & Baggaley, A. W., & Barenghi, C. F.: Knot spectrum of turbulence. *Scientific Reports*, vol. 9 no. 1: (2019).

[9] Amromin, E.: Analysis of vortex core in steady turbulent flow. *Physics of Fluids*, vol. 19 no. 11: (2007) pp. 13–16.

[10] Haller, G.: An objective definition of a vortex. *Journal of Fluid Mechanics*, vol. 525 (2005) pp. 1–26.

[11] Tropea, C. & Yarin, A., & Foss, J. F.: *Springer Handbook of Experimental Fluid Mechanics*. Springer, Heidelberg, DE (2007).

[12] Šulc, R. & Ditl, P. & Jašíkova, D. & Kotek, M. & Kopecký, V., & Kysela, B.: Effect of particle image velocimetry setting parameters on local velocity measurements in an agitated vessel. *Chemical Engineering and Technology*, vol. 42 no. 4: (2019) pp. 827–834.

[13] Koschatzky, V. & Moore, P. D. & Westerweel, J. & Scarano, F., & Boersma, B. J.: High speed piv applied to aerodynamic noise investigation. *Experiments in Fluids*, vol. 50 no. 4: (2011) pp. 863–876.

[14] Kellnerová, R. & Fuka, V. & Uruba, V. & Jurčáková, K. & Nosek, v. & Chaloupecká, H., & Jaňour, Z.: On street-canyon flow dynamics: Advanced validation of les by time-resolved piv. *Atmosphere*, vol. 9 no. 5: (2018).

[15] Uruba, V. & Pavlík, D. & Procházka, P. & Skála, V., & Kopecký, V.: On 3d flow-structures behind an inclined plate. in *EPJ Web of Conferences* vol. 143 (2017).

[16] Kurian, T. & Fransson, J. H. M.: Grid-generated turbulence revisited. *Fluid Dynamics Research*, vol. 41 no. 2: (2009) p. 021403.

[17] Pope, S. B.: *Turbulent flows*. Cambridge University Press, Cambridge, UK (2000).

[18] Duda, D. & Uruba, V.: Piv of air flow over a step and discussion of fluctuation decompositions. *AIP Conference Proceedings*, vol. 2000 (2018).

[19] Agrawal, A.: Measurement of spectrum with particle image velocimetry. *Experiments in Fluids*, vol. 39 no. 5: (2005) pp. 836–840.

[20] Duda, D. & Uruba, V.: Spatial spectrum from particle image velocimetry data. *ASME J of Nuclear Rad Sci.*, vol. 5 no. 030912: (2019).

[21] Meyer, J. & Khairy, K., & Howard, J.: Drawing an elephant with four complex parameters. *American Journal of Physics*, vol. 78 (2010) pp. 648–649.

[22] Press, W. & Teukolsky, S. & Vetterling, W., & Flannery, B.: *Numerical Recipes 3rd Edition: The Art of Scientific Computing*. Cambridge University Press (2007).

[23] Uruba, V.: Decomposition methods for a piv data analysis with application to a boundary layer separation dynamics. *Transactions of the VŠB – Technical University of Ostrava, Mechanical Series*, vol. 56 (2010) pp. 157–162.

[24] Uruba, V. & Hladík, O., & Jonáš, P.: Dynamics of secondary vortices in turbulent channel flow. in *Journal of Physics: Conference Series* vol. 318 p. 062021 (2011).

[25] Uruba, V.: Energy and entropy in turbulence decompositions. *Entropy*, vol. 21 no. 2: (2019).

[26] Holmén, V.: *Methods for Vortex Identification*. Lund University (2012). Master of Science Thesis.

[27] Kolář, V.: Vortex identification: New requirements and limitations. *International Journal of Heat and Fluid Flow*, vol. 28 no. 4: (2007) pp. 638–652.

[28] Maciel, Y. & Robitaille, M., & Rahgozar, S.: A method for characterizing cross-sections of vortices in turbulent flows. *International Journal of Heat and Fluid Flow*, vol. 37 (2012) pp. 177–188.

[29] Adrian, R. J. & Christensen, K. T., & Liu, Z.-C.: Analysis and interpretation of instantaneous turbulent velocity fields. *Experiments in Fluids*, vol. 29 no. 3: (2000) pp. 275–290.

[30] Agrawal, A. & Prasad, A.: Properties of vortices in the self-similar turbulent jet. *Experiments in Fluids*, vol. 33 no. 4: (2002) pp. 565–577.